Segregation and site selectivity in Zr-doped Y_2O_3

1997 J. Phys.: Condens. Matter 9 9731

(http://iopscience.iop.org/0953-8984/9/45/004)

J. Phys.: Condens. Matter **9** (1997) 9731–9744. Printed in the UK PII: S0953-8984(97)84920-X

Segregation and site selectivity in Zr-doped Y_2O_3

G Baldinozzi†, J-F Bérar‡, M Gautier-Soyer§ and G Calvarin†

† Laboratoire de Chimie Physique du Solide, URA CNRS 453, Ecole Centrale de Paris, F 92295 Châtenay–Malabry Cédex, France

‡ Laboratoire de Cristallographie, CNRS BP 166, F 38042 Grenoble Cédex 09, France

§ DSM/DRECAM, CEA Saclay, F 91191 Gif-sur-Yvette Cédex, France

Received 4 June 1997, in final form 28 July 1997

Abstract. High-resolution x-ray and neutron scattering studies on powder samples of pure and Zr-doped Y_2O_3 (5 at.%) show that mesoscopic compositional inhomogeneities exist in the doped compound which are unlikely to be revealed by conventional diffraction methods. Even if the structural refinement of the doped compound gives quite good reliability factors within a single-phase model, a more careful analysis of the data proves the existence of two *phases*. The main phase (90%) has a composition and a structure very close to those of pure Y_2O_3. The phase richer in Zr (10%) segregates and Zr atoms show site selectivity. The abnormally large value of the thermal displacement parameter of the site affected by the Zr substitution ($B = 4.7$ Å^2 at 294 K) is interpreted on the basis of a split-atom model characterized by an off-site displacement of 0.38 Å. Additional O atoms occupy the vacancies in the structure and provide the charge balance for the Zr dopants.

1. Introduction

Y_2O_3 crystallizes in a cubic space group ($Ia\bar{3}$) with a lattice parameter close to 10.6 Å. The unit cell contains 48 O atoms and 32 Y atoms. The atomic positions of the independent atoms are reported in table 1 (Fert 1966).

The structure is derived from the fluorite one in which each cation sits at the centre of a cube whose eight corners are occupied by anions. In Y_2O_3, only six corners of the cube (slightly distorted) are occupied by O atoms according to the symmetry of the $Ia\bar{3}$ space group. For different cationic sites, the relative positions of the two vacancies are different: for type Y_1 the vacancies stack along the face diagonal of the cube, while for type Y_2 they are along the main diagonal (figures 1 and 2). The six Y_1-O bond lengths are within the range 2.24–2.33 Å, while the six bond lengths of type Y_2-O are equal to 2.28 Å (table 4—see later).

Table 1. Atomic positions in the space group $Ia\bar{3}$; the symbol $O_\diamond$ represents the positions of anion vacancies.

Atom	Site symmetry	Multiplicity	x	y	z
O	1	48	~ 0.39	~ 0.15	~ 0.38
Y_1	$2\cdot\cdot$	24	~ 0	0	$\frac{1}{4}$
$O_\diamond$	$\cdot 3\cdot$	16	~ 0.11	~ 0.11	~ 0.11
Y_2	$\cdot\bar{3}\cdot$	8	$\frac{1}{4}$	$\frac{1}{4}$	$\frac{1}{4}$

0953-8984/97/459731+14$19.50

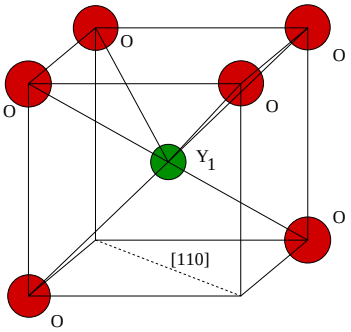

Figure 1. A schematic representation of the co-ordination of the Y_1 cation in Y_2O_3.

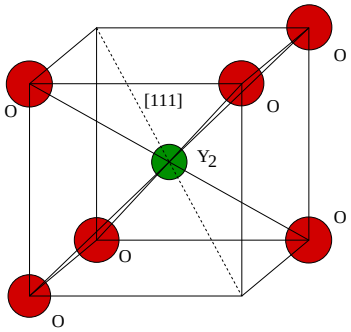

Figure 2. A schematic representation of the co-ordination of the Y_2 cation in Y_2O_3.

The room temperature crystal structure of ZrO_2 is monoclinic ($P2_1/c$) with four ZrO_2 units in the cell (Smith and Newkirk 1965). The atomic arrangement can be considered as a distortion of a fluorite structure: a Zr atom sits at the centre of the cube, five O atoms sit at the corners, and two O atoms sit in the middle of two edges. The Zr–O bond lengths are within the range 2.05–2.28 Å (table 8—see later).

ZrO_2 presents a well known monoclinic–tetragonal–cubic phase transition sequence. The relationships between the monoclinic and tetragonal phases are not straightforward as they involve a change in the coordination of Zr (from 7 to 8).

The phase diagram of the Y_2O_3–ZrO_2 system is well known for the region richer in ZrO_2. In the region of compositions richer in Y_2O_3, the occurrence of a solid solution up to a concentration of about 9 at.% ZrO_2 was reported by Duwez *et al* (1951). On the basis of an EXAFS study of a 5 at.% Zr-doped Y_2O_3 sample (Thromat *et al* 1991) it was concluded that Zr ions replace Y ions in the Y_2O_3 structure, adopting the sixfold coordination proper to Y atoms. However, the average Zr–O distance calculated (2.17 Å) is smaller than the average Y–O distance (2.26 Å) but equal to the average one in ZrO_2. From configuration interaction calculations of the yttrium and zirconium L_{II} absorption edge shapes for Y_2O_3, ZrO_2, and Zr-doped Y_2O_3, a selective substitution for Zr at the Y_2-type sites was forecast (Crocombette and Jollet 1994).

In order to prove that this site selectivity is actually exhibited, we have undertaken a structural study of a 5% Zr-doped Y_2O_3 sample by means of x-ray and neutron powder diffraction. A pure Y_2O_3 sample has also been studied for reference and comparison.

2. Experimental details

2.1. The experimental set-up

The Y_2O_3 and Zr-doped Y_2O_3 samples studied in this paper were prepared according to the method already published (Thromat *et al* 1991), and belong to the same batch of samples as were used in the earlier EXAFS study.

High-resolution x-ray powder diffraction data were collected in the laboratory using a prototype diffractometer (Bérar *et al* 1980) equipped with a copper rotating anode (18 kW) in Bragg–Brentano geometry, using a monochromatic wavelength of 1.392 17 Å. The ceramics were fixed on a flat-plate holder, and the scattering was measured with a NaI solid-state detector. The diffraction pattern was collected using variable-step scans (with care taken to ensure that there were at least five points available to define the profile lineshapes above

the half-height) and variable counting times (the scan time was increased at high angles according to the decrease of the intensity observed in the pattern). The collected data were properly merged, and each point has a weight that takes into account the effective Poissonian noise affecting each single measurement.

Neutron data were collected on the high-resolution powder diffractometer 3T2 at Laboratoire Léon Brillouin in Saclay using a monochromatic wavelength. Powders of the samples were placed in a vanadium canister and loaded into a He cryostat. The data were collected at two temperatures (294 and 8 K). As the data collection was performed using a multi-counter detector, the scheme of weighting of each point after averaging was calculated taking into account the multi-counter correction. The thermal-neutron-bound scattering lengths of Y and Zr are 7.75 and 7.16 fm respectively (Wilson 1992). The details of the data collections are summarized in table 2.

Table 2. The experimental data for Y_2O_3 and $Y_{1.90}Zr_{0.10}O_3$.

	X-ray	Neutron
Wavelength (Å)	1.392 17	1.2268
Monochromator	Graphite	Ge(335)
Step scan width, 2θ (deg)	Variable (0.01– 0.03)	0.05
2θ-range (deg)	14.0–140.0	8.0–122.0
Scan time	Variable (10–50 s)	60 000 (monitor)
Maximum counts	22 520	5427
Average background	56	133

2.2. Data analysis

Powder diffraction patterns were refined by the Rietveld method using the refinement program XND (Bérar and Garnier 1992).

The correct modelling of the Zr-doped Y_2O_3 structure depends strongly on how the full physical information contained in the patterns is extracted. Therefore, an accurate description of the profile lineshapes is needed.

In order to obtain the best results, the x-ray and neutron powder diffraction patterns were refined using Voigt functions (i.e. convolutions of Gaussian and Lorentzian functions). Previous experience has shown this to provide a very good description of high-resolution x-ray peak shapes.

The asymmetry was modelled in terms of normalized Hermitian Gaussian functions (Bérar and Baldinozzi 1993). In spite of the unavoidably high degree of correlation among some of these parameters, satisfactory convergence was obtained in all cases.

The analysis of the different Rietveld refinements performed in this paper is carried out by comparing the usual reliability factors (R_I, R_{wp}, and R_{exp}). However, when these factors are very low, one more criterion can be considered, the R_{wpc}-factor. This quantity is much more sensitive than the standard quantity R_{wp} to local correlated errors (Bérar and Le Lann 1991). The basic principle consists in an analysis of the sign of the normalized difference between the calculated and experimental profiles. If, for two contiguous points in the pattern, the sign is the same (and the product of the normalized differences is larger than a certain threshold), then the error affecting the model is considered correlated. Instead of taking the sum of the squares of the differences (the statistical error), inside the region of correlated errors the square of the sum is calculated. This reliability factor has proved

very useful in the following analysis for comparing the different structural models.

In order to exploit the specific advantages of the two experimental techniques, coupled refinements of the two data sets were performed. When x-ray and neutron refinements are coupled, attention should be paid to the statistical quality of the two data sets. In a Rietveld refinement the quantity to be minimized is the weighted sum of the squares of the differences between the experimental and calculated profiles. It is reasonable to couple the data sets only if these quantities are of the same order of magnitude for each individual data set; otherwise the weight of the set exhibiting the larger difference will dominate the refinement.

In the case of our data, this condition is well satisfied. The effect of coupling the two refinements improves the e.s.d. of the different parameters (see table 3, and table 5, later); this effect is particularly marked for the lattice parameter (the e.s.d. for the coupled refinement coincides with that of the x-ray pattern), and for the atomic and the thermal displacement parameters (the e.s.d. for the coupled refinement are close to or better of than neutron ones alone).

Table 3. The structural refinement of the neutron diffraction patterns of Y_2O_3 and Zr-doped Y_2O_3 at 294 K and 8 K in the single-phase model.

	Y_2O_3		Zr-doped Y_2O_3	
	294 K	8 K	294 K	8 K
a	10.6056(3)	10.5961(3)	10.5978(8)	10.5876(8)
$B(Y_2)$	0.44(2)	0.18(2)	0.66(3)	0.46(3)
$x(Y_1)$	−0.032 58(5)	−0.032 61(5)	−0.031 73(6)	−0.031 74(6)
$B(Y_1)$	0.43(2)	0.18(2)	0.56(2)	0.38(2)
x(O)	0.390 72(7)	0.390 75(7)	0.390 28(10)	0.390 19(10)
y(O)	0.151 90(7)	0.151 89(7)	0.151 39(10)	0.151 42(10)
z(O)	0.380 16(6)	0.380 12(6)	0.380 40(9)	0.380 33(9)
B(O)	0.48(1)	0.25(1)	0.75(2)	0.56(2)
R_{wp}	3.52	3.95	4.32	4.69
R_{wpc}	4.93	5.36	9.99	10.79
R_{exp}	2.32	2.42	2.40	2.40
G of F	1.52	1.63	1.81	1.97
R_F	1.17	1.03	2.18	1.80
R_I	1.52	1.34	3.16	2.90

3. Y_2O_3

In order to study the influence of Zr doping on the Y_2O_3 structure, we have refined, for comparison, the structure of pure Y_2O_3 using neutron data. The refined atomic positions and the isotropic thermal displacement parameters at room temperature and at 8 K are given in table 3. The results at 294 K are quite consistent with those already reported in the literature (Fert 1966). Observed, calculated, and difference plots at room temperature are shown in figure 3.

The comparison of the structural parameters at room and low temperature shows that this structure does not undergo any noticeable modification. The calculated bond lengths are reported in table 4. The Y–O average bond lengths for the two sites are almost identical (2.283 and 2.284 Å for Y_1 and Y_2 respectively). The six shortest O–O distances defining the O polyhedron centred on Y_2 are symmetry equivalent (and equal to 2.928 Å). They

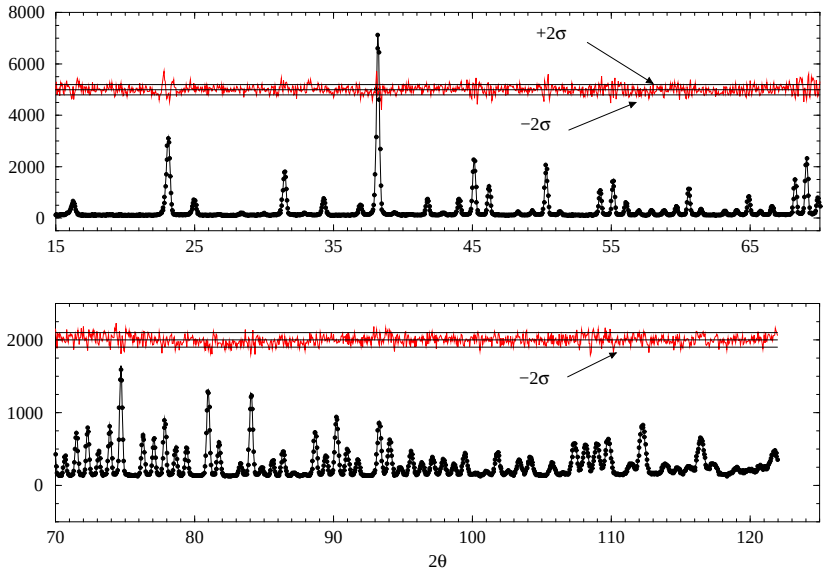

Figure 3. Observed, calculated, and difference plots for pure Y_2O_3 at 294 K.

Table 4. Bond lengths and O–O distances in Y_2O_3 at 294 K and at 8 K.

Bond	No	294 K	8 K	Distance	No	294 K	8 K
Y_1–O	2	2.245(1)	2.243(1)	O–O	2	2.906(1)	2.917(1)
Y_1–O	2	2.272(1)	2.270(1)	O–O	2	2.906(1)	2.917(1)
Y_1–O	2	2.333(1)	2.331(1)	O–O	2	2.928(1)	2.925(1)
Y_2–O	6	2.284(1)	2.282(1)	O–O	6	2.928(1)	2.925(1)

correspond to six edges of the cube in figure 2. Two of these edges are shared with a Y_1 polyhedron. The four other edges of the Y_1 polyhedron are symmetry equivalent in pairs (2.906 and 2.906 Å respectively).

4. Zr-doped Y_2O_3

The analysis of the x-ray and neutron diffraction patterns shows that all of the peaks are broadened as compared to those in the patterns for pure Y_2O_3, which can be considered almost resolution limited. As all of the data collections were performed under the same experimental conditions, these effects cannot be instrumental. Moreover, the broadening is strongly asymmetric on the higher-angle side (figure 4) and it increases at high angles. No lattice distortion of a cubic lattice can explain satisfactorily the monotonic increase of the asymmetric broadening with the θ-angle. On the other hand, this behaviour could be due to a continuous distribution of the cubic lattice parameter.

4.1. Monotonic distribution of the lattice parameters

The continuous distribution of lattice parameters has been modelled using the complex asymmetry functions detailed above. The x-ray diffraction pattern at 294 K and the neutron

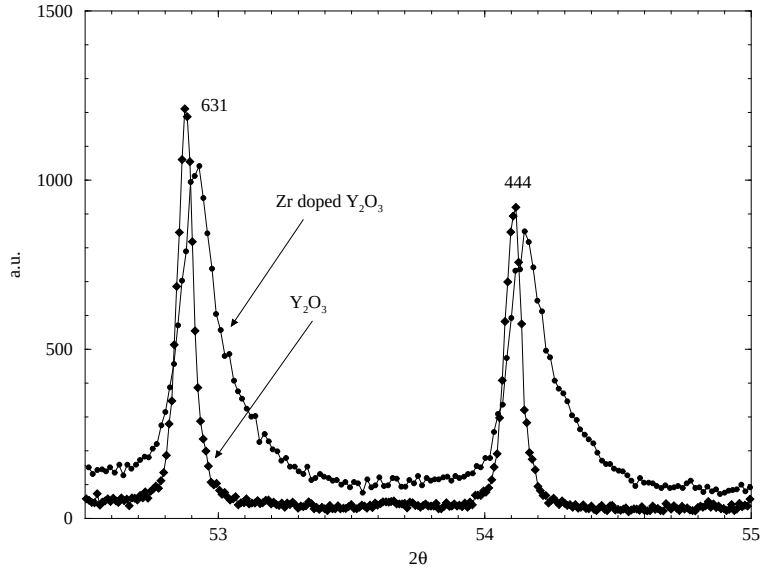

Figure 4. Comparison between the x-ray pattern of pure and doped Y_2O_3 showing the asymmetric broadening of the peak profiles.

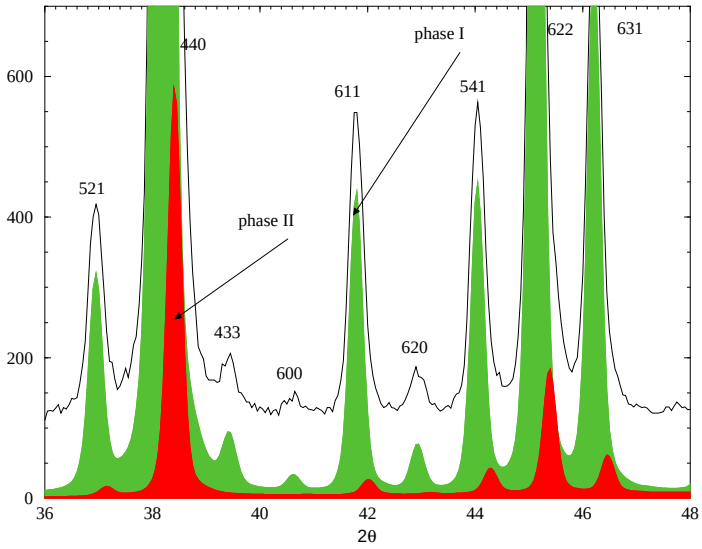

Figure 5. Modelling of the asymmetric lineshapes of the neutron powder diffraction pattern by the two symmetrical components of the bimodal distribution.

diffraction patterns at 294 K and 8 K were refined assuming a random distribution of Zr atoms over both of the cationic sites. The x-ray refinement converges to $R_{wp} = 9.11\%$ and $R_{wpc} = 23.25\%$. The results for the neutron refinements are given in table 3.

In all cases, good reliability factors are obtained, except for R_{wpc} which is very sensitive to the systematic errors affecting the modelling of the peak profiles. This means that the asymmetric broadening of the peak profile cannot be satisfactorily modelled with a

Table 5. Structural refinement results for the x-ray and neutron diffraction patterns of Zr-doped Y_2O_3 at 294 K in the biphased model. (a) Y_2^{II} sitting at the symmetry position $\cdot\bar{3}\cdot$; (b) Y_2^{II} shifted along the threefold axis [111]; (c) as (b) but with additional oxygen filling the anion vacancies. The dagger indicates the ratio (in %) of the volume of phase II to the total volume of the sample, calculated from the scale factors of the two phases. The symbols ‡, §, ‖ and ¶ are used to indicate parameters coupled during the refinement.

	(a)		(b)		(c)	
	Neutron	X-ray	Neutron	X-ray	Neutron	X-ray
a^{I}	10.5957(3)		10.5957(3)		10.5957(3)	
$B(Y_2^{I})$	0.54(2)		0.55(2)		0.53(2)	
$x(Y_1^{I})$	−0.031 68(4)		−0.031 71(4)		−0.031 75(4)	
$B(Y_1^{I})$	0.42(2)		0.42(2)		0.44(2)	
$x(O^{I})$	0.390 56(8)		0.390 53(8)		0.390 69(8)	
$y(O^{I})$	0.151 63(8)		0.151 65(8)		0.151 60(8)	
$z(O^{I})$	0.380 41(8)		0.380 39(8)		0.380 29(8)	
$B(O^{I})$	0.61(2)		0.61(2)		0.59(2)§	
$x(O_{\diamond}^{I})$	—		—		0.102(2)‖	
$p(O_{\diamond}^{I})$ (%)	—		—		2.7(4)‡	
$B(O_{\diamond}^{I})$	—		—		0.59(2)§	
a^{II}	10.5392(11)		10.5401(11)		10.5401(11)	
%†	9.8(5)		10.0(5)		10.3(5)	
$x(Y_2^{II})$	—		0.2706(9)		0.2690(10)	
$B(Y_2^{II})$	4.7(6)		0.7(3)		1.2(4)	
$x(Y_1^{II})$	−0.0214(6)		−0.0199(7)		−0.0208(6)	
$B(Y_1^{II})$	0.8(2)		1.0(2)		1.0(2)	
$x(O^{II})$	0.3814(10)		0.3806(9)		0.3844(11)	
$y(O^{II})$	0.1494(8)		0.1496(7)		0.1496(8)	
$z(O^{II})$	0.3795(10)		0.3766(10)		0.3761(11)	
$B(O^{II})$	2.0(2)		2.0(2)		2.1(2)¶	
$x(O_{\diamond}^{II})$	—		—		0.102(2)‖	
$p(O_{\diamond}^{II})$ (%)	—		—		26.4(28)‡	
$B(O_{\diamond}^{II})$	—		—		2.1(2)¶	
R_{wp}	3.83	7.90	3.80	7.83	3.59	7.71
R_{wpc}	8.00	16.91	7.62	16.40	6.05	15.56
R_{exp}	2.40	5.40	2.40	5.40	2.40	5.40
G of F	1.60	1.47	1.59	1.46	1.51	1.44
R_F^{I}	1.76	3.73	1.77	3.63	1.61	3.66
R_F^{II}	3.11	3.49	3.14	3.23	2.61	3.21
R_I^{I}	2.58	3.03	2.53	2.88	2.05	2.67
R_I^{II}	4.70	3.93	4.61	3.74	3.45	3.51

monotonic distribution of lattice parameters. So, to improve the agreement between the experimental and calculated profiles, the hypothesis of a bimodal distribution of lattice parameters was tested.

4.2. Bimodal distribution of lattice parameters

In the following, we will make reference to the two maxima of the bimodal distribution using the term *phase*. In a Rietveld refinement, all of the properties defining this *phase* correspond to those of coherent diffraction domains. The refinements have been carried out supposing that both phases are cubic with the same average symmetry ($Ia\bar{3}$); the very low reliability factors obtained for the final refinement support this hypothesis.

The coupled refinement converges satisfactorily, allowing a successful definition of the lineshapes of each of the two phases to be achieved (figure 5). The results of the structural refinement, within a random distribution model for Zr, are given in table 5, column (a). The reliability factors, especially R_{wpc}, are lowered in comparison to the values for the previous model. The main phase (I) constitutes about 90% of the sample, as can be derived from the scale factors. The lattice and the structural parameters of this phase are very close to those of pure Y_2O_3. On the other hand, the structural parameters of the second phase (II) exhibit some differences: the lattice is noticeably smaller, the O-atom coordinates are significantly changed, and the thermal displacement parameter of the cation sitting on the threefold axis is abnormally large ($B = 4.7$ Å^2).

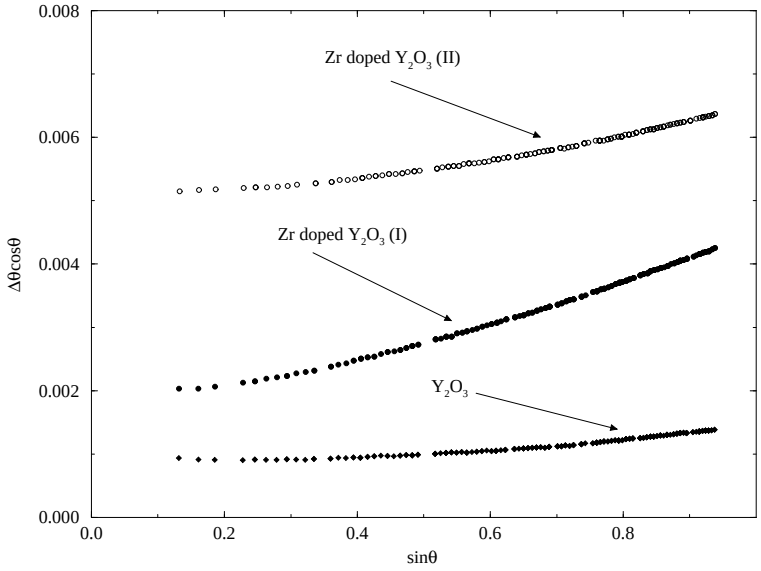

Figure 6. A Williamson–Hall plot of the evolution of the widths of the two phases for the doped compound compared to that for pure Y_2O_3. The y-intercept is 1.392 17 Å$/\delta$, δ being the x-ray crystallite size. The slope at high angles (divided by 4) gives the crystallite strain.

We have analysed the angular dependence of the x-ray lineshapes in order to obtain information about the characteristics of the two phases. Because of the high resolution of the x-ray diffraction pattern, we have been able to determine the lineshapes of each of the two phases. As can be seen in the Williamson and Hall (1953) plot of figure 6, the broadening at low angles presents a $\cos\theta$ dependence. On the other hand, the behaviour at high angles is better modelled as a $\tan\theta$ dependence. Some conclusions can be drawn from all of these results.

(i) As the refined lineshapes of the two phases are almost symmetrical, the calculated values of the lattice parameters are physically meaningful.

(ii) Each of the two phases has a lineshape much broader than that of pure Y_2O_3. The size of the coherent diffraction domains (calculated from the Scherrer relation) is much less than 1000 Å for phase II, while it is about 1000 Å for phase I.

(iii) The characteristics of this broadening are quite different: the main contribution for phase II comes from the finite crystallite size while for phase I it comes from the strain. This difference can be explained by the narrower distribution of the lattice parameter in phase II and consequently by a more homogeneous composition for this phase (this is actually confirmed by the study of the Zr selectivity and of the O stoichiometry of this phase).

All of these results show that the bimodal distribution model is more satisfactory than the monotonic distribution one, and, consequently, it was adopted in the following.

4.3. Zr segregation and site selectivity

Refinements performed with different occupancy rates of Zr dopants at the cationic sites of the two phases do not improve the reliability factors and do not change the values of the structural parameters. Therefore we have decided not to determine the effective redistribution of Zr onto the different sites directly, and a random repartition for Zr is always used in the following.

The fact that the lattice of phase II is smaller suggests that this phase is richer in Zr. Moreover, the high value of the thermal factor of the cation Y_2^{II} seems to point to the existence of a selectivity for Zr atoms at this site. To get a better description of the thermal displacement parameter of this site, a refinement was performed using an anisotropic thermal factor. The result shows that the thermal ellipsoid is not positive definite, as it becomes degenerate in a twofold hyperboloid. This result can be interpreted within a split-atom model, considering two off-site atomic positions along the threefold axis. The refinement of this model converges, and the results are presented in table 5, column (b). This model gives better reliability factors; in particular, the value of R_{wpc} is appreciably lowered. The off-site displacement of the cation Y_2^{II}, which is of about 0.38 Å, constitutes indirect evidence of site selectivity of Zr. In fact, the displacement involves the formation of three short oxygen–cation bonds (about 2.06 Å) rather different from the ones occurring in Y_2O_3 but closer to those encountered in ZrO_2 (see table 8, later). However, the number of anions in the coordination polyhedron in ZrO_2 is seven (the monoclinic phase) or eight (the tetragonal or cubic phases) instead of six as for Y_2O_3. Moreover, up to now we have not taken into account the problem of charge neutrality occurring due to the substitution of Zr^{4+} ions for Y^{3+} ions.

4.4. O stoichiometry

For these reasons we have undertaken a new series of refinements introducing additional O atoms in the vacancies of the Y_2O_3 structure (16*c*). As the doped compound contains 5% of Zr^{4+}, 5% of the vacancies must be filled by O to balance the charges. The $Ia\bar{3}$ average symmetry imposes a random filling. The positions of this atom were taken to be the same for the two phases, and the sum of the occupancy rates of $O_\diamond$ in each of the two phases has been constrained to respect the total charge balance. Therefore, only two additional parameters were introduced in this model. Whatever the starting values of the $O_\diamond$ occupancy rates are for the two phases, the refinement is well conditioned, and a successful convergence is always obtained. The reliability factors of the two phases are noticeably improved—in particular, those affecting the neutron diffraction pattern which is the most sensitive to the O stoichiometry, witnessing the physical significance of this parameter (table 5, column

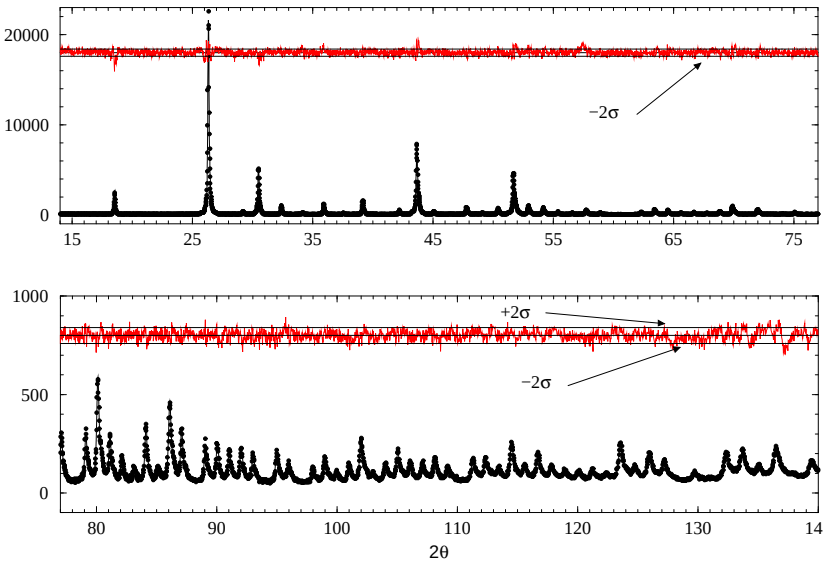

Figure 7. Observed, calculated, and normalized difference plots for Zr-doped Y_2O_3 at 294 K (x-ray diffraction patterns).

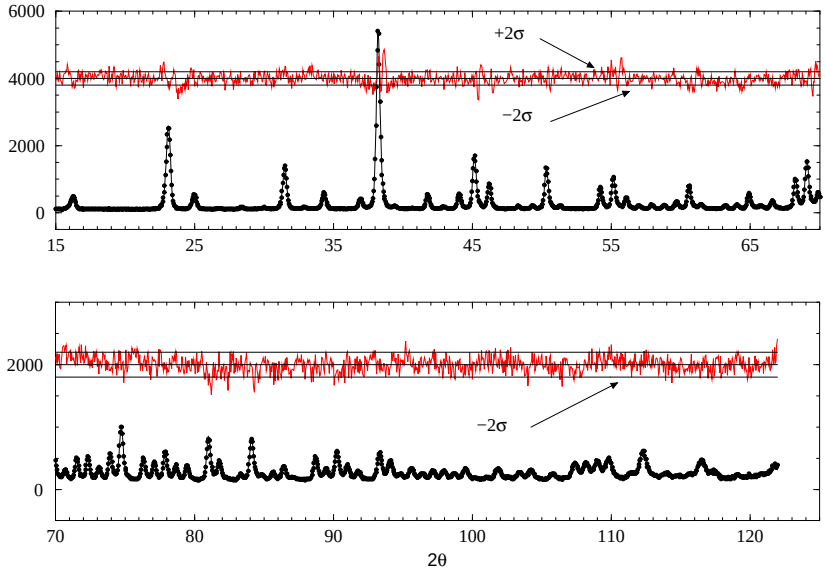

Figure 8. Observed, calculated, and normalized difference plots for Zr-doped Y_2O_3 at 294 K (neutron diffraction patterns).

(c)). The additional O atoms fill 2.7% and 26% of the vacancies in phase I and phase II respectively. Observed, calculated, and difference plots at 294 K are shown in figures 7 and 8.

The same refinement sequence was performed at 8 K on the neutron diffraction pattern, the rate of phase II being fixed at the value obtained at room temperature. The results are

Table 6. Structural refinement results for the neutron diffraction pattern of Zr-doped Y_2O_3 at 8 K in the biphased model. (a) Y_2^{II} sitting at the symmetry position $\cdot\bar{3}\cdot$, (b) Y_2^{II} shifted along the threefold axis [111]; (c) as (b) but with additional oxygen atoms filling the anion vacancies. The symbols †, ‡, §, ‖ and ¶ are used to indicate parameters coupled during the refinement.

	(a)	(b)	(c)
a^{I}	10.5818(7)	10.5818(7)	10.5818(7)
$B(Y_2^{I})$	0.32(3)	0.32(3)	0.30(3)
$x(Y_1^{I})$	−0.031 92(6)	−0.031 92(6)	−0.031 99(6)
$B(Y_1^{I})$	0.24(2)	0.25(2)	0.27(2)
$x(O^{I})$	0.390 35(8)	0.390 33(8)	0.390 45(8)
$y(O^{I})$	0.151 45(9)	0.151 48(9)	0.151 47(8)
$z(O^{I})$	0.380 37(8)	0.380 34(8)	0.380 27(7)
$B(O^{I})$	0.40(2)	0.41(2)	0.37(2)§
$x(O_\diamond^{I})$	—	—	0.104(2)‖
$p(O_\diamond^{I})$ (%)	—	—	2.3(4)‡
$B(O_\diamond^{I})$	—	—	0.37(2)§
a^{II}	10.516(2)	10.517(2)	10.518(2)
$x(Y_2^{II})$	0.25	0.270(2)	0.270(2)
$B(Y_2^{II})$	5.5(9)	1.9(2)†	1.9(2)†
$x(Y_1^{II})$	−0.018(1)	−0.017(1)	−0.018(1)
$B(Y_1^{II})$	1.8(2)	1.9(2)†	1.9(2)†
$x(O^{II})$	0.379(2)	0.378(2)	0.384(2)
$y(O^{II})$	0.149(1)	0.149(1)	0.149(1)
$z(O^{II})$	0.381(2)	0.379(2)	0.379(2)
$B(O^{II})$	2.3(2)	2.4(2)	2.4(2)¶
$x(O_\diamond^{II})$	—	—	0.104(2)‖
$p(O_\diamond^{II})$ (%)	—	—	30.2(29)‡
$B(O_\diamond^{II})$	—	—	2.4(2)¶
R_{wp}	3.92	3.89	3.69
R_{wpc}	7.29	7.21	6.13
R_{exp}	2.40	2.40	2.40
G of F	1.65	1.64	1.56
R_F^{I}	1.36	1.36	1.19
R_F^{II}	3.38	3.31	2.79
R_I^{I}	2.20	2.20	1.78
R_I^{II}	4.85	4.30	3.16

given in table 6. As for the refinements at 294 K, the reliability factors strongly decrease when additional O atoms are introduced in the split-atom model. The values of the off-site displacement for Y_2^{II} and of the percentages of $O_\diamond$ in the two phases are in good agreement with the ones determined at room temperature. This good agreement constitutes independent evidence of the reliability of the proposed structural model.

The bond lengths in Zr-doped Y_2O_3, calculated using the final model, are given in table 7. In phase I, the distances Y_1-O and Y_2-O are equal to the ones occurring in pure

Table 7. Bond lengths in Zr-doped Y_2O_3 at 294 K and at 8 K.

Bond	Phase	No	294 K	8 K
Y_1-O	I	2	2.237(1)	2.238(1)
Y_1-O	I	2	2.272(1)	2.268(1)
Y_1-O	I	2	2.333(1)	2.326(1)
Y_2-O	I	6	2.284(1)	2.280(1)
Y_1-O	II	2	2.220(11)	2.184(15)
Y_1-O	II	2	2.292(10)	2.309(14)
Y_1-O	II	2	2.357(11)	2.352(15)
Y_2-O	II	3	2.083(12)	2.092(16)
Y_2-O	II	3	2.385(15)	2.402(23)

Table 8. Bond lengths in monoclinic ZrO_2 (according to Smith and Newkirk 1965) and in tetragonal ZrO_2 (according to Patil and Subbarao 1970).

Bond	No	Monoclinic	Bond	No	Tetragonal
$Zr-O_1$	1	2.051	$Zr-O_1$	4	2.065
$Zr-O_1$	1	2.057	$Zr-O_2$	4	2.455
$Zr-O_1$	1	2.163			
$Zr-O_2$	1	2.151			
$Zr-O_2$	1	2.189			
$Zr-O_2$	1	2.220			
$Zr-O_2$	1	2.285			

Y_2O_3. In phase II, the six Y_1-O distances are almost unchanged while the six $Y_2^{II}-O$ distances are split into two sets of three short and three long distances (2.083 and 2.385 Å respectively at 294 K). The values of the short distances are almost equal to those occurring in ZrO_2 (table 8). The distance between the O atoms and the centre of the ideal cube surrounding the cations is unchanged for Y_1 but it is appreciably shortened for Y_2 (from 2.284 Å to 2.212 Å). This isotropic contraction of the O polyhedron shows unambiguously that a large degree of substitution of Zr for Y atoms occurs on the latter site.

5. Discussion

The Rietveld refinements of the x-ray and neutron powder diffraction patterns at 294 K and at 8 K of the 5% Zr-doped Y_2O_3 sample show that the bimodal distribution of lattice parameters improves the description of all of the diffraction patterns, as is witnessed by all of the reliability factors. Moreover, the structural and chemical characteristics obtained for both *phases* are fully consistent: the main phase exhibits structural features close to those of the Y_2O_3, while phase II (about 10%) presents some specific differences that are attributed to the selective substitution of Zr.

The direct determination of the Zr repartition in the two phases is not possible because of the weak contrast between Y and Zr atoms. On the other hand, an indirect determination can be made on the basis of the quantity of additional O found in each phase. The substitution rate of Zr for Y cations, which has to be equal to the substitution rate of O for vacancies, is about 2.7 and 26% in phase I and phase II respectively. These values confirm that phase II is much more heavily doped but, as this phase constitutes only 10% of the sample, only about half of the total number of dopants are substituted into this phase. The second half

are found in phase I.

A selective substitution of Zr for Y occurs at the site Y_2^{II}. This result is deduced from the structural features of the cation at this site: the off-site displacement of 0.38 Å associated with a contraction of the O polyhedron gives rise to short cation–oxygen bond lengths similar to those occurring in ZrO_2 phases.

Let us examine the influence of Zr substitution on the Y_2O_3 framework. The contraction of the O polyhedron centred on the Y_2 cation results in a shortening of O–O distances from 2.928 to 2.782 Å. The two distances shared with Y_1 polyhedra decrease too, inducing structural defects. When the density of defects reaches a critical threshold (2.7% of the atomic substitution from our results), a phase segregation takes place. This value is much smaller than the limit of solid solution of ZrO_2 in Y_2O_3 (9 at.%) determined by Duwez *et al* (1951) from macroscopic measurements.

If the substitution occurs only on the Y_2 sites, which represent 25% of the total cationic sites, the limit of solubility of Zr in Y_2O_3 (2.7%) corresponds to a substitution rate of 10.8% at this site. At higher Zr concentrations, the system is biphased. As the calculated value for the Zr substitution rate in the second phase is 26%, this phase should correspond to a well defined compound with chemical formula $Y_3ZrO_{6.5}$. The average structure of this compound is probably close to that of phase II. In fact, the refinements at low temperature (8 K) exhibit rather large thermal displacement parameters. This suggests that, in spite of the very good reliability factors obtained, the real symmetry of this phase is probably slightly different from that of pure Y_2O_3.

This work illustrates how high-resolution diffraction experiments performed on a real material allow us to demonstrate and characterize the occurrence of compositional inhomogeneities in polycrystalline samples that standard x-ray experiments are unlikely to reveal. In the sample studied, *phase II*, which constitutes 10% of the total, is probably dispersed in the solid solution (*phase I*), and the size of the coherent diffraction domains is less than 1000 Å. The coexistence of the two phases could be responsible of the modifications observed in the mechanical properties for the doped samples (Gautier 1997). High-resolution electron microscopy experiments could establish precisely the microstructure of phase II in the matrix and describe the interactions. A study of anomalous scattering using synchrotron radiation may enhance the contrast between the atomic scattering factors of Y and Zr, leading to a better description of the structural features of phase II.

References

Bérar J F and Baldinozzi G 1993 *J. Appl. Crystallogr.* **26** 128
Bérar J F, Calvarin G and Weigel D 1980 *J. Appl. Crystallogr.* **13** 201
Bérar J F and Garnier P 1992 *Accuracy in Powder Diffraction II: Proc. Int. Conf. (NIST Special Publication No 846)* ed E Prince and J K Stalick (Gaithersburg, MD: US Department of Commerce, NIST)
Bérar J F and Le Lann P 1991 *J. Appl. Crystallogr.* **24** 1
Crocombette J P and Jollet F 1994 *J. Phys.: Condens. Matter* **6** 8341
Gautier M 1997 unpublished results
Duwez P, Brown F H and Odell F 1951 *J. Electrochem. Soc.* **98+99** 356
Fert A 1966 *Bull. Soc. Fr. Miner. Crist.* **89** 194
Patil R N and Subbarao E C 1970 *Acta Crystallogr.* A **26** 535
Smith D K and Newkirk H W 1965 *Acta Crystallogr.* **18** 983
Thromat N, Noguera C, Gautier M, Jollet F and Durand J P 1991 *Phys. Rev.* B **44** 7904
Williamson G K and Hall W H 1953 *Acta Metall.* **1** 22
Wilson A J C 1992 *International Tables for Crystallography* vol C (Dordrecht: Kluwer)